8-30-2023

Molecular dynamics simulation of interfacial tension of the CO2-CH4-water and H2-CH4-water systems at the temperature of 300 K and 323 K and pressure up to 70 MPa

Quoc Truc Doan
Edith Cowan University

Alireza Keshavarz
Edith Cowan University

Caetano R. Miranda

Peter Behrenbruch

Stefan Iglauer
Edith Cowan University

10.1016/j.est.2023.107470
Doan, Q. T., Keshavarz, A., Miranda, C. R., Behrenbruch, P., & Iglauer, S. (2023). Molecular dynamics simulation of interfacial tension of the CO2-CH4-water and H2-CH4-water systems at the temperature of 300 K and 323 K and pressure up to 70 MPa. *Journal of Energy Storage*, 66, Article 107470.
https://doi.org/10.1016/j.est.2023.107470

Journal of Energy Storage 66 (2023) 107470

Contents lists available at ScienceDirect

Journal of Energy Storage

journal homepage: www.elsevier.com/locate/est

Research papers

Molecular dynamics simulation of interfacial tension of the CO_2-CH_4-water and H_2-CH_4-water systems at the temperature of 300 K and 323 K and pressure up to 70 MPa

Quoc Truc Doan [a,*], Alireza Keshavarz [a], Caetano R. Miranda [b], Peter Behrenbruch [c], Stefan Iglauer [a]

[a] Centre for Sustainable Energy and Resources, Edith Cowan University, 270 Joondalup Drive, Joondalup 6027, Western Australia, Australia
[b] Departamento de Física dos Materiais e Mecânica, Instituto de Física, Universidade de São Paulo, São Paulo 05508-090, São Paulo, Brazil
[c] Bear and Brook Consulting, 135 Hilda Street, Corinda, Brisbane, Queensland 4075, Australia

ARTICLE INFO

Keywords:
Hydrogen geo-storage
Underground Hydrogen Storage (UHS)
Interfacial tension
Carbon Capture and Storage (CCS)
Molecular dynamics simulation
Depleted hydrocarbon reservoirs

ABSTRACT

Subsurface geologic formations such as depleted hydrocarbon reservoirs, deep saline aquifers and shale formations have been considered promising targets for carbon dioxide and hydrogen storage. A solid understanding of the interfacial properties of multiphase systems, including binary (pure gas-water) and ternary (gas mixtures and water), is vital to assess for reliability and storage capacity of the geological formations. However, most previous experimental and simulation studies for interfacial properties have mainly focused on binary systems at low-medium pressure. Only a few experimental and simulation studies investigated the interfacial tension at high pressure (above 20 MPa) for the CO_2-CH_4-H_2O system, and no simulation data are available for the H_2-CH_4-H_2O system. In this study, Molecular dynamics simulations were used to predict the interfacial tension (γ) for both the binary and ternary system at 300 K and 323 K for a wide pressure range (1.0 to 70 MPa). The study was first conducted for the binary systems (H_2O-CO_2; H_2O-CH4 and H_2O—H_2) and then followed by the ternary systems (CO_2-CH_4-H_2O and H_2-CH_4-H_2O). The γ results were also validated with previous studies by comparing them to experimental and simulation data. The findings of this study indicated that γ data of binary and ternary systems decreased with increasing pressure and temperature. However, at high pressure (above 50 MPa), the γ data at 300 K and 323 K showed a plateau or changed very slightly, apparently not depending significantly on temperature. Furthermore, at a fixed pressure, determined γ values for the ternary system (H_2-CH_4-H_2O) are constantly larger than for the CH_4-H_2O and CO_2-CH_4-H_2O systems. The results provide extending or new γ data in simulation for the binary and ternary systems and contribute to evaluating the stability and long-term viability of various key Carbon Capture and Storage (CCS) and Underground Hydrocarbon Storage (UHS) related processes in support of the large-scale implementation of a hydrogen economy.

1. Introduction

With the global population and economic growth, world energy consumption is based mainly on fossil fuels such as coal, oil and natural gas [1]. However, Carbon Dioxide (CO_2) emissions from fossil fuel consumption have been identified as the main cause of global warming and remain a challenge in reaching the goals of the Paris Agreement [2]. To deal with this problem, there are many technological solutions, including implementing Carbon Capture and Storage (CCS) and renewable energy sources [3,4]. While CCS provides an effective means to reduce greenhouse gas emissions in fossil fuel power plants and carbon-intensive industries [5,6], energy storage from renewable energy sources in the form of Hydrogen (H_2) is considered a promising solution to provide clean fuel and replace traditional fossil fuels to reduce emissions of CO_2 [7,8].

Depleted hydrocarbon reservoirs, deep saline aquifers and shale formations have been identified as potential geological targets to inject and store CO_2 or H_2 into underground formations for CCS projects and hydrogen geo-storage, also called Underground Hydrogen Storage (UHS) [9,10]. There are three main reasons for selecting subsurface formations for injection [11]. Firstly, subsurface data of the geological

* Corresponding author.
E-mail address: t.doan@ecu.edu.au (Q.T. Doan).

https://doi.org/10.1016/j.est.2023.107470
Received 20 February 2023; Received in revised form 12 April 2023; Accepted 15 April 2023
Available online 27 April 2023

Nomenclature

γ	interfacial tension
θ	contact angle
r	effective capillary (or pore) radius
CCS	Carbon Capture and Storage
EPM2	Elementary Physical Models
MD	molecular dynamics
NVT	canonical ensemble
NPT	isothermal-isobaric ensemble
NIST	National Institute of Standard and Technology
OPLS	optimized potentials for liquid simulations
P	pressure
P_c	capillary pressure
PPPM	particle-particle-particle-mesh
T	temperature, absolute
TIP4P	transferable intermolecular potential with four points for water
UHS	Underground Hydrocarbon Storage

of the γ studies for binary and ternary systems and the range of thermo-physical conditions. It can be seen from Table 1 that most studies of the binary system (CO_2-H_2O and CH_4-H_2) have been conducted at 275.15 to 398.15 K and up to 50 MPa. However, only two experimental studies [23,26] were performed for the H_2-H_2O system. Furthermore, little γ data [20,21,29,37] are available for the ternary system (CO_2-CH_4-H_2O) at high pressure, and only γ data from experiment [38] is available for the (H_2-CH_4-H_2O) system. Note that these ternary systems are of vital importance as gas reservoirs may also contain CO_2 [39,40] and that it is furthermore possible that microorganisms convert the H_2 into CO_2 or CH_4 [41,42]. It is also possible that CH_4 is used as a cushion gas for maintaining reservoir pressure during storage [43], or that unprocessed gas, e.g., directly from steam reforming [44] is injected.

In this study, Molecular dynamics simulation studies were used to predict the interfacial tension (γ) for both the binary and ternary system at 300 K and 323 K for a wide pressure range (1.0 to 70 MPa). Firstly, the simulation was conducted for the binary systems (H_2O-CO_2; H_2O-CH_4 and H_2O—H_2) and then followed by the ternary systems (CO_2-CH_4-H_2O and H_2-CH_4-H_2O). The predicted γ results were also validated with previous studies by comparing them to experimental and simulation data. The obtained results provide extending or new γ data in simulation for both the binary and ternary systems. The benefits of this study

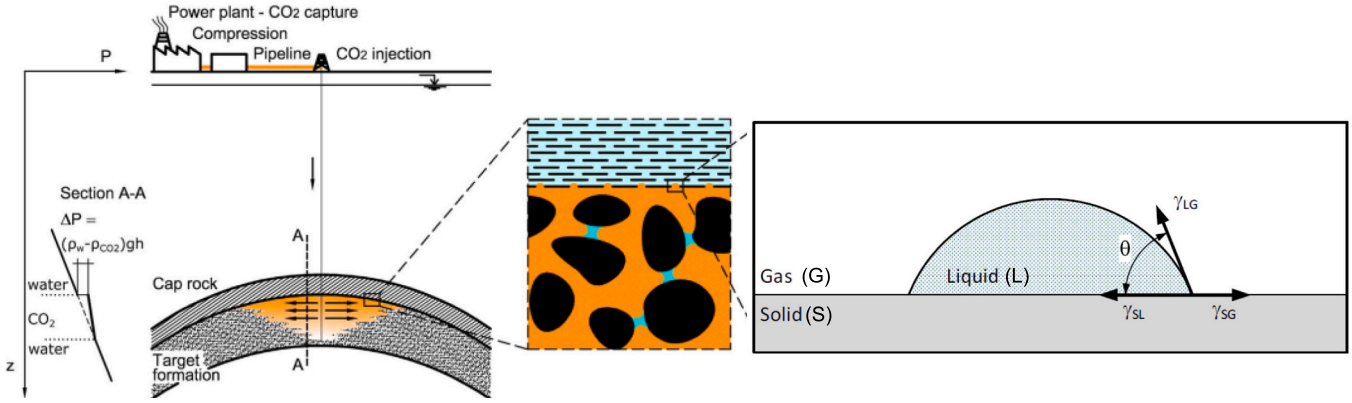

Fig. 1. An illustration of interfacial properties impacts on reliability and storage capacity for CCS and UHS projects [15,16].

formations have been collected and studied during the exploration and production stages. Secondly, the underground and surface infrastructure (wells, equipment and pipelines) already exist and could be reused for storage projects with minor or without modification [11]. Thirdly, the practice of injecting different gases into oil and gas reservoirs for enhanced recovery has been successfully mastered by the petroleum industry. Lessons learned are valuable in extending the practice to H_2/CO_2 injection for sequestration purposes.

The reliability and storage capacity of a storage formation or oil/gas field is strongly controlled by capillary pressure [12–14], as quantified by the Young-Laplace Eq. (1)

$$P_c = P_g - P_w = \frac{2\gamma\cos\theta}{r} \quad (1)$$

where P_c is the capillary pressure across the interface of two fluids as a function of the fluid-fluid interfacial tension γ, contact angle θ, and effective capillary (or pore) radius r as shown in Fig. 1. The formula indicates that γ is one of the key parameters determining how much gas can be stored and how the gas plume spreads in the subsurface [17,18]. It is, therefore, necessary to study the interfacial tension of such water-H_2/CO_2 gas mixtures in detail.

A number of experimental studies ([19–28]) and simulation studies ([29–36]) have been carried out to measure or predict the γ data of various gas-water systems in the past decade. Table 1 summarizes some

contribute to evaluating the stability and long-term viability of various key Carbon Capture and Storage (CCS) and Underground Hydrocarbon Storage (UHS) and support the implementation of large-scale CCS and UHS to decarbonize the energy supply chain.

This study is organized as follows: Section 2 describes the molecular models and MD simulation methods in detail. The simulation results are presented and discussed in Section 3 and a summary and conclusion can be found in Section 4.

2. Simulation methods

In this study, molecular dynamics simulation was performed using the open-source LAMMPS package [45] to calculate interfacial tension (γ), including CO_2/H_2O, CO_2/CH_4/H_2O, H_2/H_2O and H_2/CH_4/H_2O-γ at a wide pressure range (1 to 70 MPa). Simulated results are also compared to experimental data from previous studies.

2.1. Force fields

A group of mathematical functions calculating the energy for a specified atomic configuration is called a force field ([46,47]). A typical force field may have the following potential energy terms:

$$U_{total} = U_{coul} + U_{vdw} + U_{stretch} + U_{bend} \quad (2)$$

Table 1
Experimental and simulation data for water-gas interfacial tension of studied binary and ternary systems.

Authors	Year	Method	Systems	Pressure, MPa	Temperature, K
Naeiji et al.	2020	Simulation	CO_2/CH_4/H_2O	4–10	275.15 and 298.15
Chen et al.	2019	Simulation	CO_2/CH_4/H_2O	3–20	323.15
Yang et al.	2019	Simulation	CO_2/CH_4/H_2O (Brine)[c]	Up to 60	348
Yang et al.	2017	Simulation	CO_2/CH_4/H_2O (Brine)[a]	Up to 60	311–473
Nair et al.	2022	Simulation	CO_2/CH_4/H_2O (Brine)[c]	Up to 100	311–473
Lui et al.	2016	Experiment	CO_2/CH_4/H_2O (Brine)[b]	0.1–34.7	298.15 and 398.15
Ren et al.	2000	Experiment	CO_2/CH_4/H_2O	1–3	298–373
Chow et al.	2020	Experiment	H_2/H_2O	0.5–45	298 to 448
Massoudi et al.	1974	Experiment	H_2/H_2O	7.6	298.15
Silvestri et al.	2019	Simulation	CO_2/H_2O	1–50	308, 323 and 383
Li et al.	2013	Simulation	CO_2/H_2O (Brine)[b]	2–50	303 and 393
Stefan et al.	2012	Simulation	CO_2/H_2O	1–20	300, 343 and 350
Nielsen et al.	2012	Simulation	CO_2/H_2O	3–30	300–383
Georgiadis et al.	2010	Experiment	CO_2/H_2O	1–60	298–374
Chiquet et al.	2007	Experiment	CO_2/H_2O	5–45	308–383
Kvamme et al.	2007	Experiment	CO_2/H_2O	0.1–20	278–335
Hebach et al.	2002	Experiment	CO_2/H_2O	0.1–20	278–335
Naeiji et al.	2019	Simulation	CH_4/H_2O	Up to 10	275.15 and 298.15
Khosharay et al.	2014	Experiment	CH_4/H_2O & CO_2/H_2O	0.1–6	284.15–312.15
Sachs et al.	1995	Experiment	CH_4/H_2O	0.5–46.8	298.15
Mirchi et al.	2022	Experiment	H2/CH4/H2O (Brine)[a]	6.9	295.15, 313.15 and 333.15

[a] Brine is from NaCl.
[b] Brine including Na^+, Ca^{2+} and Cl^-.
[c] Brine includes NaCl or $CaCl_2$.

where U_{coul} is the Coulombic interaction, U_{vdw} is the Van der Waals intermolecular potential, $U_{stretch}$ is the bond stretching potential and U_{bend} is bond angle bending potential.

The Coulombic interactions are calculated according to Coulomb's law [47]:

$$U_{coul} = \frac{q_i q_j}{4\pi\varepsilon_o r_{ij}^2} \tag{3}$$

where q_i and q_j are the partial charges of atoms i and j, ε_o is the permittivity of free space, and r_{ij} is the distance between the atoms.

The van der Waals intermolecular potential force (non-bonded) can be described by the Lenard-Jones (L-J) potential [48],

$$U_{vdw} = 4\varepsilon_{ij}\left[\left(\frac{\sigma_{ij}}{r_{ij}}\right)^{12} - \left(\frac{\sigma_{ij}}{r_{ij}}\right)^{6}\right] \tag{4}$$

where ε_{ij} is the well depth for short-range interactions, σ_{ij} are core diameter for the L-J potential and r_{ij} is the distance between atoms.

Table 2
Lennard Jones and Coulombic interaction parameters.

Molecule model	Atom	Mass (g/mol)	ε (kcal/mol)	σ (Å)	q (e)
H_2O	H	1.00800	0.0000	0.000	0.520
(TIP4P/2005)	O	15.9994	0.1852	3.159	−1.040
CO_2	C	12.0110	0.0559	2.757	0.651
(EPM2)	O	15.9994	0.1597	3.033	−0.326
CH_4	C	12.0110	0.0660	3.500	−0.240
(OPLS)	H	1.00800	0.0300	2.500	0.060
H_2[a]	H	1.00800	0.0198	0.272	0.740

[a] [52].

For the van der Waals interaction parameters between unlike atoms, the Lorentz Berthelot mixing rule was applied as follows [47]

$$\sigma_{ij} = \left(\sigma_{ij} + \sigma_{ij}\right)\Big/2 \text{ and } \varepsilon_{ij} = \sqrt{\varepsilon_{ij}\varepsilon_{ij}} \tag{5}$$

The intramolecular interactions contain bond stretching and bond angle bending defined by a harmonic potential. The bond stretching potential is given by:

$$U_{stretch} = K_r(r - r_0)^2 \tag{6}$$

And the bond angle bending potential is defined by the following:

$$U_{bend} = K_\theta(\Phi - \Phi_0)^2 \tag{7}$$

where r, r_0, Φ and Φ_0 represent the measured bond length, the equilibrium bond length, the measured angle and the equilibrium angle. K_r and K_θ are the bond stretching and angle bending force constants, respectively [29].

In this study, the TIP4P/2005 force field [49] was used to model water, while the EPM2 force field [50] was selected for the CO_2 model; the OPLS force-field [51] was used for CH_4 and H_2 models using the parameters proposed by Yang and Zhong [52]. The force-field parameters used are given in Table 2.

2.2. Simulation methodology

The simulation approach in previous studies was followed [53,54] by equilibrating the simulation boxes separately before combining them, as shown in Fig. 2. In the first step, a simulation cell size of 3.2 nm × 3.2 nm × 3.2 nm was generated through a bulk phase MD simulation at 300 K and 323 K, and the gas (CO_2, CH_4 and H_2) pressure was modified by varying the number of gas molecules in the box. A total of 1088 water molecules were used for each simulation. Periodic boundary conditions were applied in three dimensions in all simulations [29,55], and energy minimization was performed prior to the simulations [29,53]. The initial velocity distribution of the molecules used the Maxwell-Boltzmann distribution [29]. The cut-off radius was set to 10 Å (less than half of the minimum three-dimensional size) for both the Lennard-Jones and long-range non-bonded electrostatic interactions. For the long-range Coulombic interactions, a particle-particle-particle-mesh (PPPM) method was applied with an expected relative error in forces of 0.0001 [29]. For the force field TIP4P/2005, the SHAKE [56,57] algorithm was used with a relative tolerance of 0.0001, to constrain the bond length and angle of water molecules, allowing a longer time step. The timestep was 0.5 fs to calculate the nonbonded interactions. The temperature and pressure were fixed using a Nose-Hoover thermostat and barostat. The simulations were run under an NPT ensemble for 5 ns to obtain density values close to the experimental values from NIST database [58]. In particular, the NP_zT ensemble was used to allow simulation box expansion or contraction [29,54], limited to the z-direction (x-length and the y-length were held constant). As a result, the z-length of the gas box changed in a range of 3.2 nm to 4.1 nm depending on pressure, while the z-length of the H_2O box changed slightly to around 3.2 nm. In the second step, a rectangular box with H_2O in the middle and gas (CO_2,

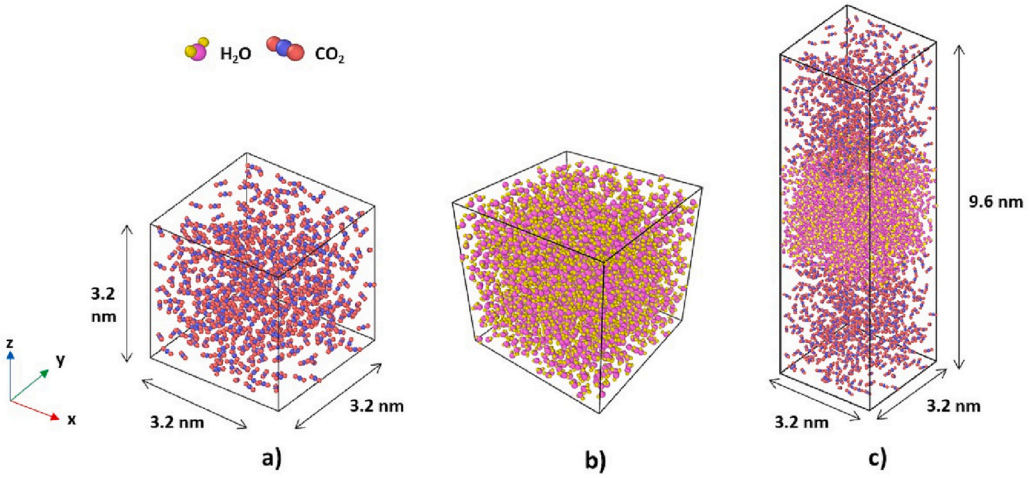

Fig. 2. An example of the initial configuration for individual simulation boxes; a) bulk CO_2, b) bulk H_2O, and c) a mixed CO_2-H_2O system.

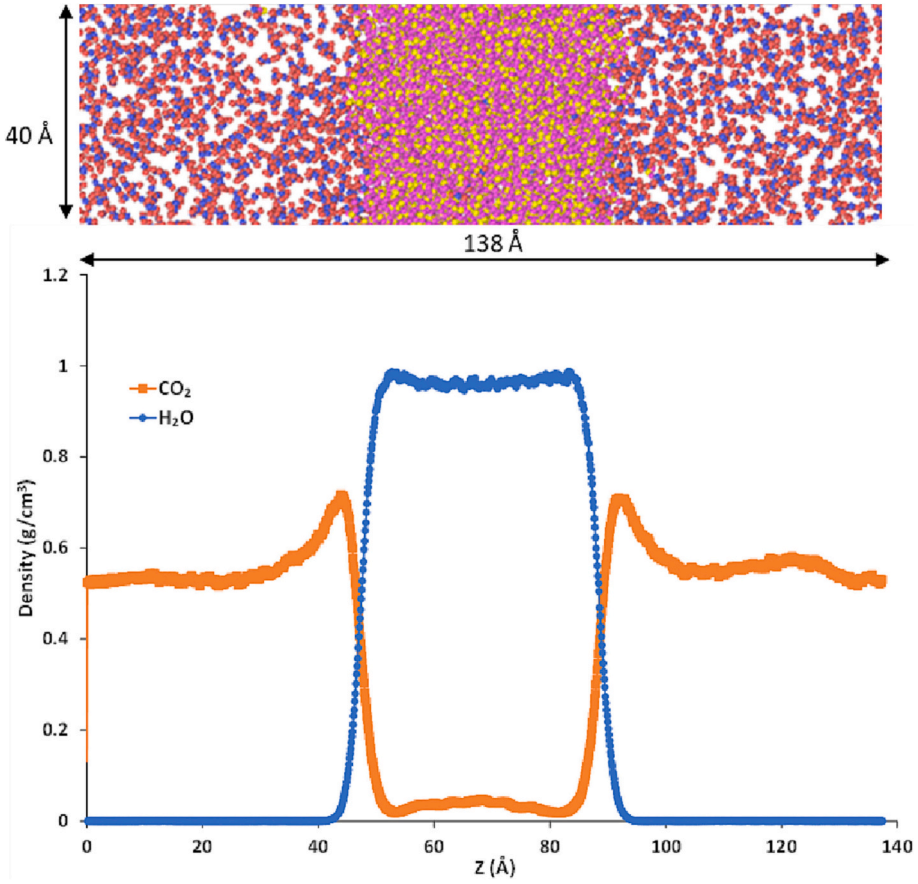

Fig. 3. Final snapshot of the CO_2/water system simulation box at 300 K and 7 MPa.

CH_4 and H_2) on both sides were combined, ready to determine interfacial properties. The number of gas molecules ranged from 8 to 515, depending on pressure, while the number of water particles was fixed at 1088 molecules. The system equilibrated at 300 K and 5 MPa for 5.5 ns under the NVT ensemble. The last 5 ns of simulations was considered a production step to collect data to calculate the results, see Fig. 3. Production steps were applied to five blocks for calculating interfacial tension (γ), including error bars.

2.3. Interfacial tension

The surface/interfacial tension, γ, for the water and gas/water systems can be obtained by the following equation.

$$\gamma = \gamma_{sim} + \gamma_{tc} \tag{8}$$

where γ_{sim} is the surface/interfacial tension calculated using the mechanical approach [59], with the diagonal components of the pressure tensor normal to the surface given by:

Table 3
γ(CO_2-water), γ(CH_4-water) and γ(H_2-water) at 300 K and 323 K as a function of pressure. The standard error is shown in parentheses.

Temperature	Pressure	γ (mN/m)		
(K)	*(MPa)*	*CO_2-H_2O*	*CH_4-H_2O*	*H_2-H_2O*
300	1	62.1 (0.6)	64.3 (0.7)	62.8 (0.4)
	5	55.5 (0.9)	59.5 (0.8)	63.8 (0.4)
	10	38.0 (1.1)	58.4 (0.9)	64.1 (0.3)
	20	36.7 (1.0)	55.9 (0.9)	62.4 (1.1)
	50	34.6 (0.9)	54.0 (1.1)	62.3 (0.6)
	70	34.0 (0.7)	53.1 (0.3)	62.2 (0.9)
323	1	58.3 (0.3)	59.6 (0.5)	60.3 (0.6)
	5	52.6 (0.4)	57.1 (0.7)	59.6 (0.8)
	10	43.5 (0.6)	56.8 (0.9)	59.5 (0.5)
	20	36.4 (1.0)	53.8 (1.0)	59.7 (0.6)
	50	34.2 (0.7)	50.6 (0.4)	60.7 (0.7)
	70	32.2 (0.6)	50.9 (1.1)	59.6 (0.5)

$$\gamma_{sim} = \frac{L_z}{2}\left(P_{zz} - \frac{P_{xx} + P_{yy}}{2}\right) \tag{9}$$

where L_z is the system length along the z-axis, and P_{xx}, P_{yy} and P_{zz} are the components of the pressure tensor.

γ_{tc} is the tail correction, which accounts for the effect of truncating intermolecular potentials. γ_{tc} is calculated [60] as follows:

$$\gamma_{tc} = 12\pi \sum_{a}^{N} \sum_{b}^{N} \varepsilon_{ab}\, \sigma_{ab}^{6}\, x \int_{-\infty}^{+\infty} \int_{-1}^{1} \int_{r_c}^{\infty} \rho_a(z_1)\rho_b(z_r - 1)\frac{1 - 3s^2}{r^4} dr ds dz_1 \tag{10}$$

where $\rho_a(z)$ is the density profile of molecule a along the z-direction, r_c is the cut-off radius, N is the number of distinct molecule types in the simulation, z_1 and z_2 are the z-axis coordinates of molecules 1 and 2, respectively, and $s = (z_1 - z_1)/r$.

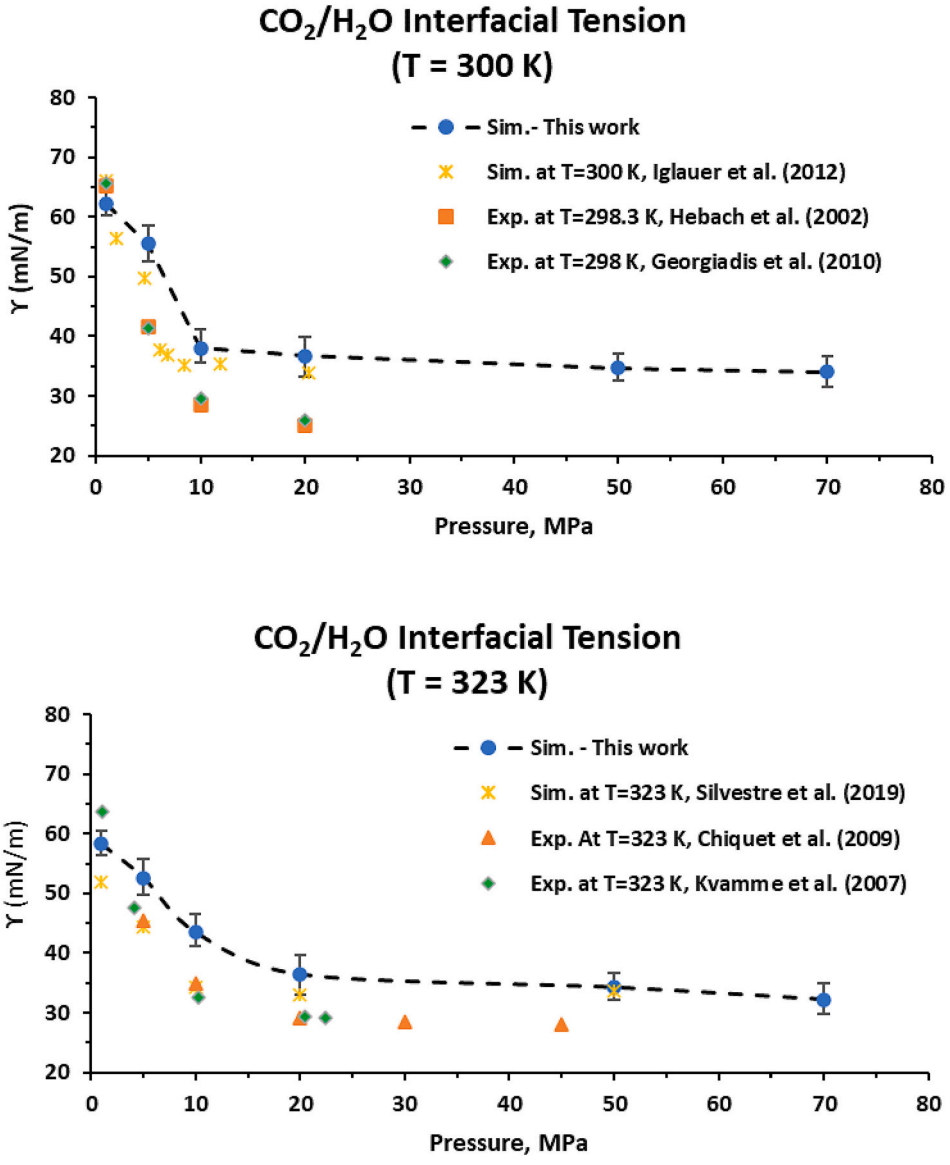

Fig. 4. γ((CO_2-H_2O) as a function of pressure and temperature, experimental and simulation data.

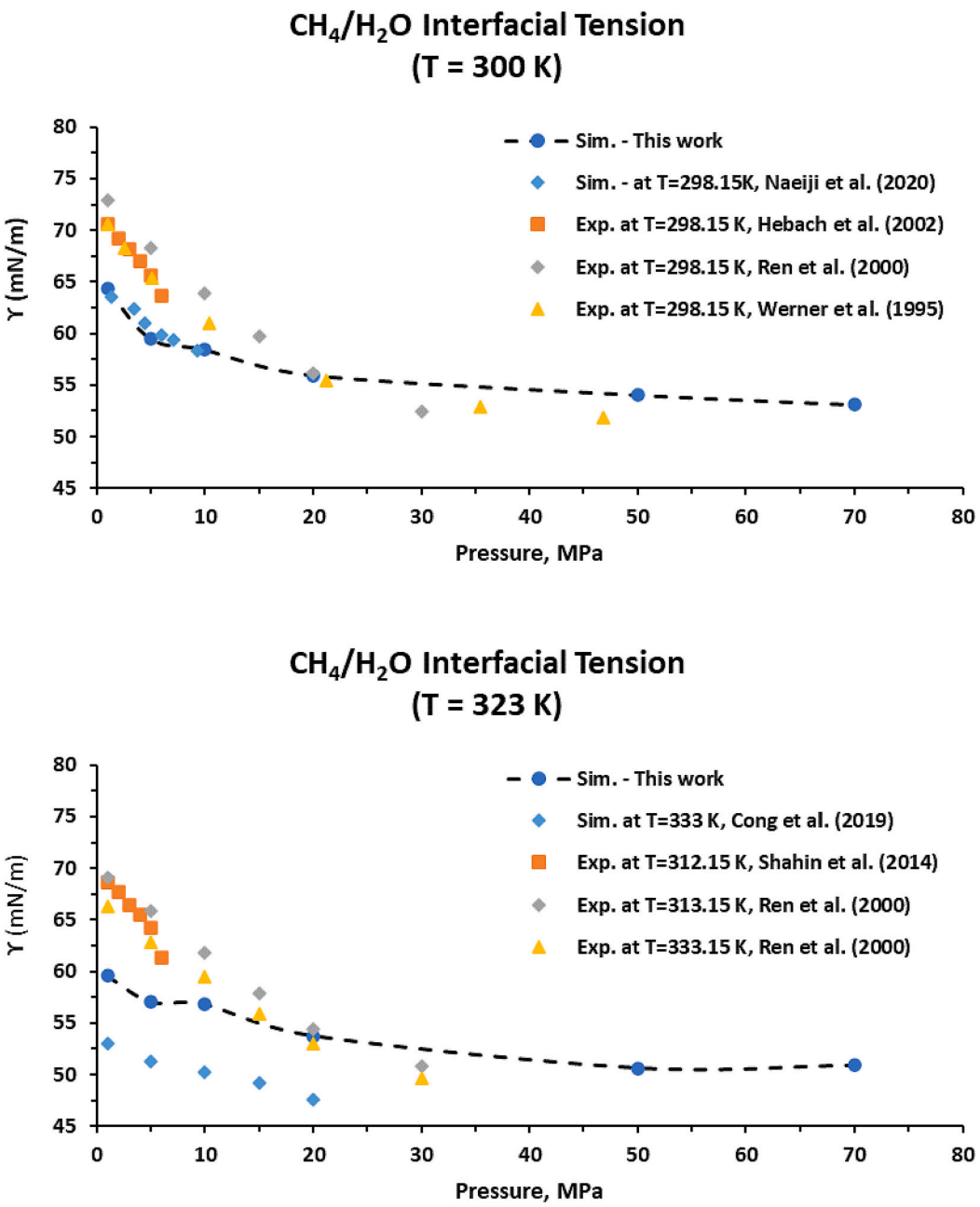

Fig. 5. $\gamma(CH_4\text{-}H_2O)$ as a function of pressure and temperature, experimental and simulation data.

3. Results and discussion

3.1. Interfacial tension for binary systems (H_2O-CO_2, H_2O-CH_4 and H_2O—H_2)

The calculated interfacial tension of pure carbon dioxide-, methane- and hydrogen-water systems under different 300 K and 323 K and a wide range of pressures of 1 MPa to 70 MPa are summarized in Table 3. The calculated results are compared to experimental and molecular dynamics simulation. The results of the simulations presented in this study agree with previous studies and are documented experimental errors.

γ (CO_2-H_2O) as a function of pressure and temperature is shown in Fig. 4, where it is also compared with experimental results ([19,24]; and [25]) and previous simulation results [30]. The simulated results (with a standard error of around 1.0) are in good agreement with previous simulation data in low and high-pressure regions. In contrast, with pressure below the critical pressure (around 7.0 MPa), there is a significant difference with experiment data (around 9 mN/m), which can be caused by selecting forefield models [33], using the Lorentz-Berthelot combining rules [30] and the size of simulation box [31]. At high pressure (above 50 MPa), the γ data at 300 K and 323 K are constant or changed very slightly, indicating no or little dependence on temperature.

$\gamma(CH_4\text{-}H_2O)$ results of this study, as a function of pressure and temperature, are shown in Fig. 5, indicating good agreement with the previous simulation studies [32]. However, the simulated $\gamma(CH_4\text{-}H_2O)$ was lower than experimental values at lower pressure (by less than 10 %), although the agreement improved as pressure increased above 20 MPa. At high pressure (above 50 MPa), the γ data at 300 K and 323 K reaches a constant value or plateau, behaving similar to the CO_2-H_2O system. However, at the same pressure, the $\gamma(CH_4\text{-}H_2O)$ requires higher pressure to reach a constant value when compared to the $\gamma(CO_2\text{-}H_2O)$.

$\gamma(H_2\text{-}H_2O)$ was found to generally decrease slightly with increasing pressure but was found to decrease strongly with increasing

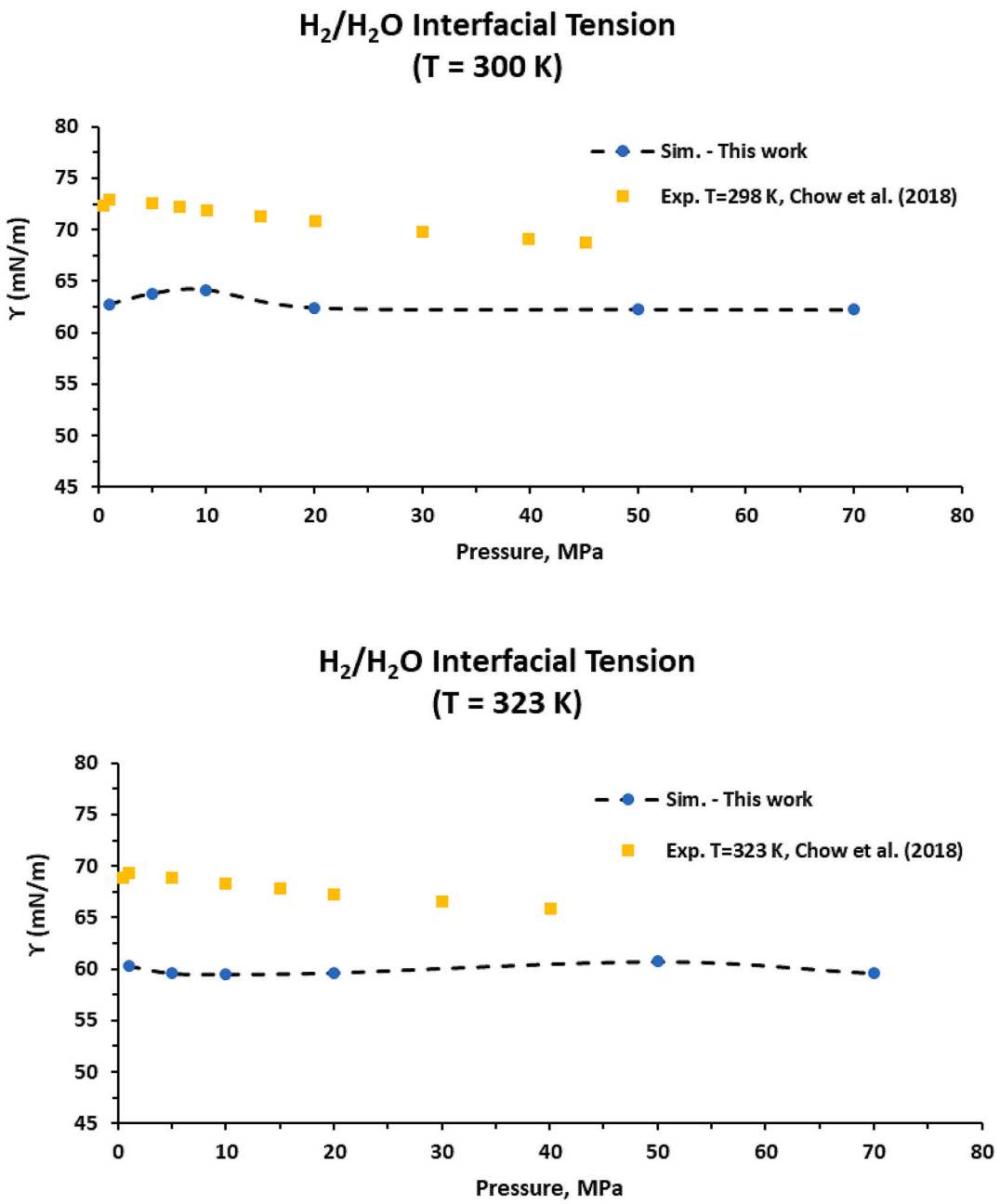

Fig. 6. $\gamma(H_2\text{-}H_2O)$ as a function of pressure and temperature, experimental and simulation data.

temperature, as shown in Fig. 6. Simulated results show a similar trend in comparison with the experimental results [23], but γ simulated values are underestimated by about 10–14 % when compared with experimental data [23]. At present there is no published information for simulation data of $\gamma(H_2\text{-}H_2O)$ for validation. The differences between simulated and experiment results in $\gamma(H_2\text{-}H_2O)$ may possibly be explained by the degree of accuracy in the description of the force field [33] or using the Lorentz-Berthelot combining rules [30]. Besides, [31] mentioned that the difference can be due to other simulation parameters such as the size of simulation box.

γ of the binary systems decreases with increasing pressure and temperature, Fig. 7. At constant pressure, H_2 exhibited the highest γ value, while CO_2 had the lowest γ. This result can be explained by presenting the number of molecules adsorbed (or intermolecular forces) at the interface [36]. At the same temperature, the $\gamma(CH_4\text{-}H_2O)$ requires higher pressure to reach a constant value or plateau compared to the $\gamma(CO_2\text{-}H_2O)$, attributed to a rate of increased adsorption of CO_2 molecules at the surface, higher when compared with CH_4 [36].

3.2. *Interfacial tension of ternary systems (CO_2-CH_4-H_2O and H_2-CH_4-H_2O)*

The simulated interfacial tension of CO_2-CH_4-H_2O and H_2-CH_4-H_2O under different thermodynamic conditions is listed in Table 4. The gas mixture composition was chosen to give an approximate 60:40 mol ratio for CO_2:CH_4 and H_2:CH_4 as this composition is comparable to that used in experiments [21] and also simulations [32,61]. However, for the H_2-CH_4-H_2O system, no published simulation data could be found and only experiment data [38] at $P = 6.9$ MPa.

Interfacial tension calculated for the carbon dioxide-methane-water system is shown in Fig. 8. The results agree with previous simulation work [32]. Simulated results are lower than experimental values [21] by about 10 % when the pressure is at 10 MPa. The agreement improves as increasing pressures above 10 MPa. At high pressures (above 50 MPa), γ

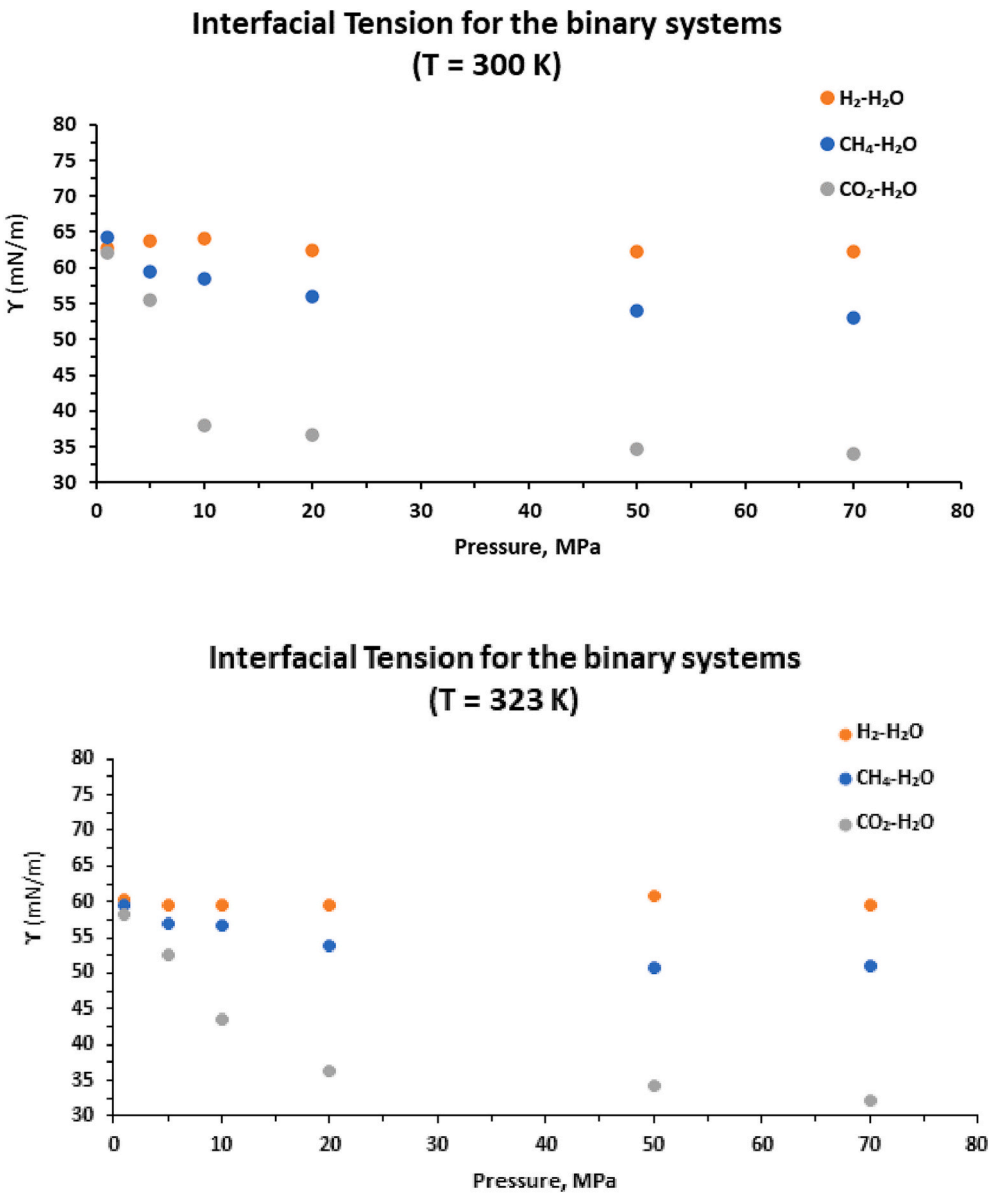

Fig. 7. Interfacial tension γ of the (H_2O-CO_2, H_2O-CH_4 and H_2-H_2O systems at 300 K and 323 K as a function of pressure, simulation data.

Table 4
Predicted γ(CO_2-CH_4-water) at 323 K and γ(H_2-CH_4-water) at 300 K as a function of pressure. The standard error is shown in parentheses.

P	γ (mN/m) at $T = 323$ K		P	γ (mN/m) at $T = 300$ K	
(MPa)	*CH_4-H_2O*	*CO_2-CH_4-H_2O*	*(MPa)*	*CH_4-H_2O*	*H_2-CH_4-H_2O*
1	59.6	58.7 (0.5)	1	64.3	63.9 (1.1)
5	57.1	54.7 (0.6)	5	59.5	62.8 (0.7)
10	56.8	52.9 (0.6)	10	58.4	61.7 (1.0)
20	53.8	48.0 (0.8)	20	55.9	59.0 (0.9)
50	50.6	43.9 (0.6)	50	54.0	55.8 (1.1)
70	50.9	43.1 (0.8)	70	53.1	55.9 (0.8)

remained unchanged. Furthermore, γ decreased with increasing pressure, Fig. 9. However, the γ values of the CO_2-CH_4-H_2O system are lower than the CH_4-H_2O system at fixed pressure or temperature. The lower γ values are caused by the presence of CO_2 in the CO_2-CH_4-H_2O system, consistent with previous studies [32,34]. The cause is due to stronger intermolecular interaction of CO_2 molecules with the H_2O molecules at the interface.

As expected, γ(H_2-CH_4-water) decreased with increasing pressure, similar to γ(CH_4-H_2O). The γ result is in good agreement in comparison with previous experimental study at $P = 6.9$ MPa [38] At high pressure (above 50 MPa), γ(H_2-CH_4-water) remained unchanged, similar to results for the CO_2-CH_4-H_2O system. Furthermore, at constant pressure, the predicted γ was higher than the γ for the CH_4-H_2O and CO_2-CH_4-H_2O systems, as shown in Fig. 10 and Fig. 11. Results show that γ increased with the presence of H_2, which leads to a decrease in the number of absorbed CH_4 molecules at the surface [41], and also intermolecular interactions of H_2 with H_2O molecules at the surface are less strong when compared with CO_2 or CH_4.

Here, although the extended and new γ data results from this study conducted at a wider range of pressure (1.0 MPa to 70 MPa) and showed a similar trend in comparison with previous experimental and simulation studies for the binary and ternary system. But there is limited data available on the system of H_2-H_2O and H_2-CH_4-H_2O for validating the predicted results and significant differences between this study's simulation data and previous experimental data. Therefore, further improvements in the future may be conducted by using different force field models (CO_2, CH_4, H_2) when combing with the water model or varying

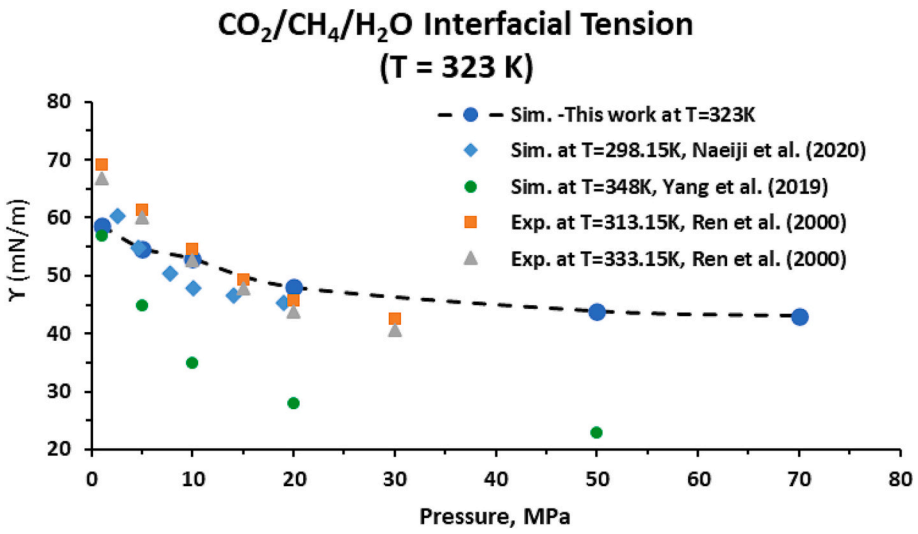

Fig. 8. $\gamma(CO_2\text{-}CH_4\text{-}H_2O)$, experimental and simulation data.

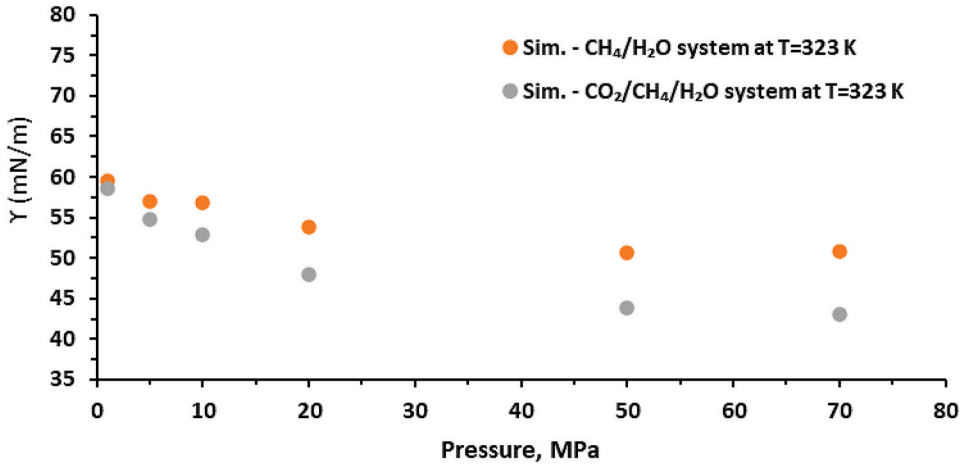

Fig. 9. A comparison of $\gamma(CH_4/H_2O)$ and $\gamma(CO_2/CH_4/H_2O)$.

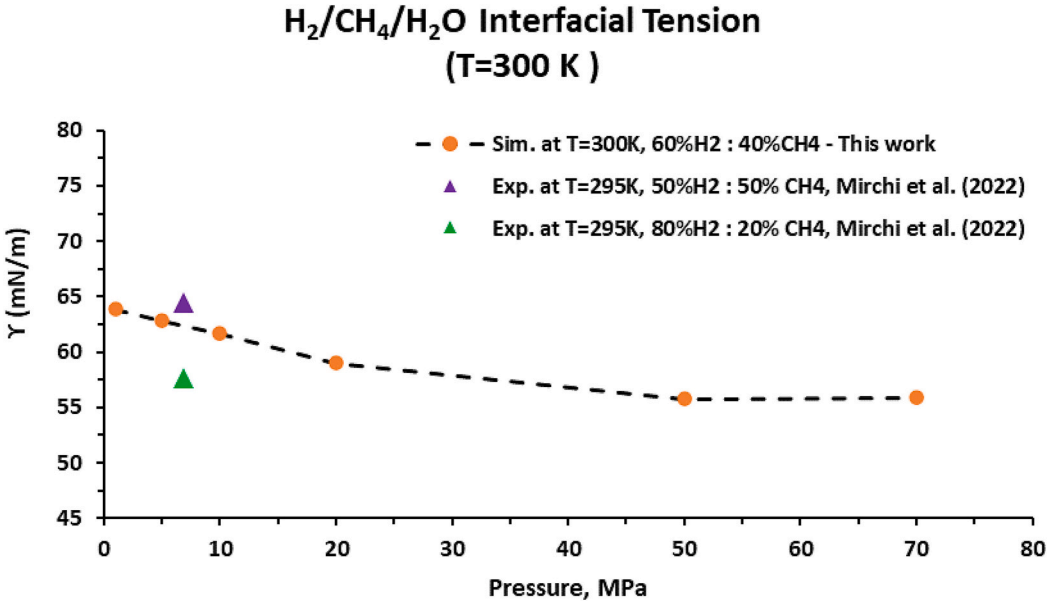

Fig. 10. $\gamma(H_2\text{-}CH_4\text{-}H_2O)$ predicted as a function of pressure (at 300 K).

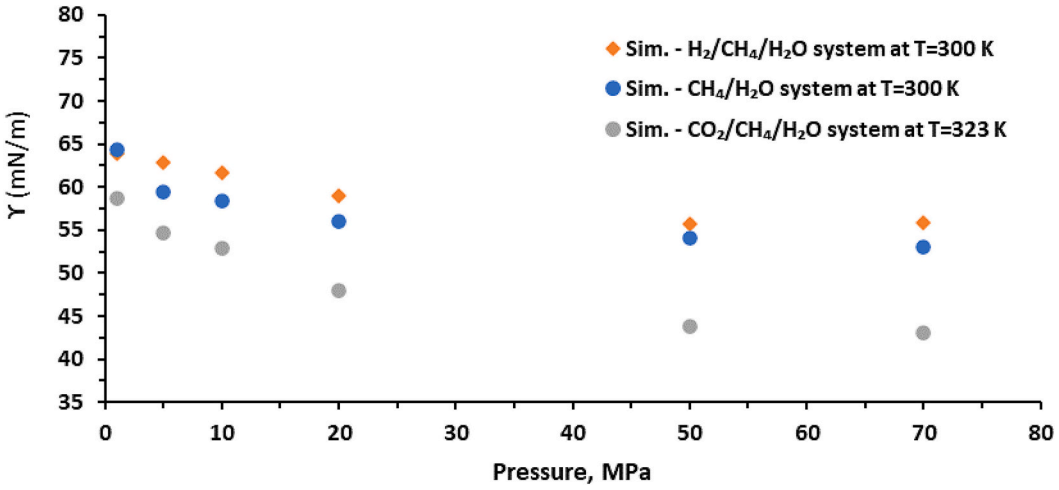

Fig. 11. A comparison of $\gamma(CH_4/H_2O)$, $\gamma(CO_2/CH_4/H_2O)$ and $\gamma(H_2/CH_4/H_2O)$.

sizes of simulation boxes to investigate impacts on the γ data and also expect to reduce the gap of the differences.

4. Summary and conclusions

1. The interfacial tension (γ) of the binary (pure gas-water) and ternary (gas mixtures and water) systems is vital for the evaluation of the storage capacity of CO_2 or H_2 in depleted hydrocarbon reservoirs, deep saline aquifers and shale formations.
2. This study summaries methodologies and a workflow for deriving values for γ, the key parameter required for various CCS- and UHS-related processes, in support for the implementation of a large-scale hydrogen economy.
3. In reviewing prior publications relevant to the presented study, several shortcomings were identified. Firstly, experimental and simulated results for the determination of γ have been limited to pressure levels above 20 MPa for the CO_2-CH_4-H_2O system. Secondly, for the H_2-CH_4-H_2O system no published γ data could be found.
4. To extend the applicability of diverse gas injection scenarios reported previously, simulations of this study were aimed at validating previous experimental and simulation results and developing previous work. Molecular dynamics simulations were performed to predict interfacial tension (γ) for various binary (H_2O-CO_2; H_2O-CH_4 and H_2O—H_2) and ternary (CO_2-CH_4-H_2O and H_2-CH_4-H_2O) systems at 300 K and 323 K and a wide pressure range (1.0 to 70 MPa).
5. For binary and ternary systems, γ values were generally found to decrease with both, increasing pressure and temperature. However, at high pressure (above 50 MPa), γ data at 300 K and 323 K indicated an unchanged or very weakly fluctuating response, with temperature change having little influence. Furthermore, at the same pressure, the γ value of the ternary system (H_2-CH_4-H_2O) in the presence of H_2 is improved or increased compared with the binary system (CH_4-H_2O) and also the ternary system (CO_2-CH_4-H_2O).
6. The results provide extending or new γ data in simulation for the binary and ternary systems and contribute to evaluating the stability and long-term viability of various key Carbon Capture and Storage (CCS) and Underground Hydrocarbon Storage (UHS) related processes in support of the large-scale implementation of a hydrogen economy.

Declaration of competing interest

Quoc Truc Doan reports financial support was provided by Bear and Brook Consulting. Stefan Iglauer reports financial support was provided by Australian Research Council.

Data availability

Data will be made available on request.

Acknowledgements

This research was supported by Bear and Brook Consulting and the Australian Government through the Australian Research Council's Discovery Projects funding scheme (project DP220102907). The authors would also like to thank the Pawsey Supercomputing Centre for providing supercomputing time and resources.

References

[1] I. Yildiz, 1.12 fossil fuels, in: Comprehensive Energy Systems, Elsevier, Amsterdam, 2018, pp. 521–567.
[2] Adoption of the Paris Agreement, Proposal by the President, in: Conference of the Parties Twenty-first Session, Paris, 2015.
[3] A. Azzuni, C. Breyer, Energy security and energy storage technologies, 2018, Energy Procedia 155 (2018) 237–258. ISSN 1876-6102.
[4] CSIRO, National Hydrogen Roadmap – Pathways to an Economically Sustainable Hydrogen Industry in Australia, 2018.
[5] M.J. Blunt, C.H. Pentland, R. El-Magrhaby, S. Iglauer, CO2 sequestration in sandstones and carbonates, in: Qatar Petroleum and Shell-Imperial College Grand Challenge Collaborative Programme on Clean Fossil Fuels Progress Meeting, London, UK, 26th January 2011, 2011.
[6] D. Zivar, S. Kumar, J. Foroozesh, 2020, Underground hydrogen storage: a comprehensive review, Int. J. Hydrog. Energy (2020), https://doi.org/10.1016/j.ijhydene.2020.08.138.
[7] B. Pan, X. Yin, Y. Ju, S. Iglauer, Underground hydrogen storage: influencing parameters and future outlook, Adv. Colloid Interface Sci. 294 (2021), 102473.
[8] R. Tarkowski, Underground hydrogen storage: characteristics and prospects, Renew. Sust. Energ. Rev. 105 (2019) 86–94.
[9] N. Heinermann, M.G. Booth, R.S. Haszeldine, M. Wilkinson, J. Scafidi, K. Edlmann, Hydrogen storage in porous geological formations onshore play opportunities in the midland valley (Scotland, UK), Int. J. Hydrog. Energy 2018 (2018) 20861–20874.
[10] D.R. Simbeck, 2004, CO2 capture and storage—the essential bridge to the hydrogen economy, Energy 29 (9–10) (2004) 1633–1641. ISSN 0360-5442.
[11] Z. Li, M. Dong, S. Li, S. Huang, 2006, CO2 sequestration in depleted oil and gas reservoirs—caprock characterization and storage capacity, Energy Convers. Manag. 47 (11–12) (2006) 1372–1382.
[12] S. Iglauer, C.H. Pentlan, A. Busc, CO2 wettability of seal and reservoir rocks and the implications for carbon geo-sequestration, Water Resour. Res. 51 (1) (2014) 729–774, https://doi.org/10.1002/2014WR015553.
[13] S. Iglauer, Dissolution Trapping of Carbon Dioxide in Reservoir Formation Brine – A Carbon Storage Mechanism. 2011, 2011.
[14] S. Iglauer, 2017, CO2–water–rock wettability: variability, influencing factors, and implications for CO2 geostorage, Acc. Chem. Res. 50 (5) (2017) 1134–1142.
[15] A. Abramov, A. Keshavarz, S. Iglauer, Wettability of quartz surfaces under carbon dioxide geo-sequestration conditions. A theoretical study. https://ro.ecu.edu.au/theses/2232, 2019.

[16] D.N. Espinoza, J.C. Santamarina, CO2 breakthrough-caprock sealing efficiency and integrity for carbon geological storage, Int. J. Greenh. Gas Control 66 (2017) (2017) 218–229.

[17] Vialle S. Al-Khdheeawi, A. Barifcani, M. Sarmadivaleh, S. Iglauer, Impact of reservoir wettability and heterogeneity on CO2-plume migration and trapping capacity, EA Int. J. Greenh. Gas Control 58 (142–158) (2017) 2017.

[18] S. Iglauer, Optimum geological storage depths for structural H2 geo-storage S, J. Pet. Sci. Eng. 212 (2022), 109498.

[19] A. Georgiadis, G. Maitland, J.P.M. Trusler, A. Bismarck, 2010, Interfacial tension measurements of the (H2O+CO2) system at elevated pressures and temperatures. J. Chem. Eng. Data 2010, 55, 4168-4175 Calculating geological storage, Energy Convers. Manag. 50 (2) (February 2009) 431.

[20] Y. Liu, H.A. Li, R. Okuno, 2016, Measurements and modeling of interfacial tension for CO2/CH4/brine systems under reservoir conditions, Ind. Eng. Chem. Res. 55 (48) (2016) 12358–12375, https://doi.org/10.1021/acs.iecr.6b02446.

[21] Q.Y. Ren, G. Chen, W. Yan, T. Guo, 2000, Interfacial tension of (CO2 + CH4) + water from 298 K to 373 K and pressures up to 20 MPa, J. Chem. Eng. Data 45 (4) (2000) 610–612, https://doi.org/10.1021/je990301s.

[22] P. Chiquet, J.L. Daridon, D. Broseta, S. Thibeau, CO_2/water interfacial tensions under pressure and temperature conditions of CO_2 geological storage, Energy Conversion Management 48 (3) (2007) 736–744, https://doi.org/10.1016/j.enconman.2006.09.011.

[23] Y.F. Chow, G.C. Maitland, J.P.M. Trusler, Interfacial tensions of (H2O + H2) and (H2O + CO2 + H2) systems at temperatures of (298–448) K and pressures up to 45 MPa, Fluid Phase Equilib. 503 (1 January 2020) (2018) 112315.

[24] A. Hebach, A. Oberhof, N. Dahmen, A. Kogel, H. Edere, E. Dinjus, 2002, Tension at elevated pressures-measurements and correlations in the water + carbon dioxide system, J. Chem. Eng. Data 47 (2002) 1540–1546.

[25] B. Kvamme, T. Kuznetsova, A. Hebach, A. Oberhof, E. Lunde, Measurements and modelling of interfacial tension for water + carbon dioxide systems at elevated pressures, Comput. Mater. Sci. 38 (2007) (2007) 506–513.

[26] R. Massoudi, A.D.J. King, 1974, Effect of pressure on the surface tension of water. Adsorption of low molecular weight gases on water at 25°, J. Phys. Chem. 78 (1974) 2262–2266.

[27] K. Shahin, V. Farshad, 2014, Experimental and modeling investigation on surface tension and surface properties of (CH4+H2O), (C2H6+H2O), (CO2+H2O) and (C3H8 + H2O) from 284.15 K to 312.15 K and pressure up to 60 bar, Int. J. Refrig. 47 (2014) 26–35.

[28] S. Werner, M. Volker, 1995, Pressure and temperature dependence of the surface tension in the system natural gas/water. Principles of investigation and the first precise experimental data for pure methane/water at 25oC up to 46.8 MPa, Colloids Surf. A Physicochem. Eng. Asp. 94 (1995) 291–301.

[29] C. Chen, W. Hu, W. Li, Y. Song, 2019, Model comparison of the CH4/CO2/water system in predicting dynamic and interfacial properties, J. Chem. Eng. Data 64 (6) (2019) 2464–2474, https://doi.org/10.1021/acs.jced.9b00006.

[30] S. Iglauer, M.S. Mathew, F. Bresme, 2012, Molecular dynamics computations of brine-CO2 interfacial tensions and brine-CO2-quartz contact angles and their effects on structural and residual trapping mechanisms in carbon geo-sequestration, J. Colloid Interface Sci. 386 (1) (2012) 405–414.

[31] X. Li, D.A. Ross, J.P.M. Trusler, G. Maitland, E.S. Boek, 2013, Molecular dynamics simulations of CO2 and brine interfacial tension at high temperatures and pressures, J. Phys. Chem. B 117 (18) (2013) 5647–5652, https://doi.org/10.1021/jp309730m.

[32] P. Naeiji, T.K. Woo, S. Alavi, R. Ohmura, 2020, Molecular dynamics simulations of interfacial properties of the CO2-water and CO2-CH4-water systems, J. Chem. Phys. 153 (2020), 044701, https://doi.org/10.1063/5.0008114.

[33] A. Silvestri, E. Ataman, A. Budi, S.L. Stipp, J.D. Gale, P. Raiteri, 2019, Wetting properties of the CO2-water-calcite system via molecular simulation: shape and size effects, Langmuir 35 (50) (2019) 16669–16678, https://doi.org/10.1021/acs.langmuir.9b02881.

[34] Y. Yafan, N. Narayanan, K. Arun, S. Sun, Molecular dynamics simulation study of carbon dioxide, methane and their mixture in the presence of brine, J. Phys. Chem. B 121 (41) (2017) 9688–9698, https://doi.org/10.1021/acs.jpcb.7b08118.

[35] L.C. Nielsen, I.C. Bourg, G. Sposito, 2012, Predicting CO2–water interfacial tension under pressure and temperature conditions of geologic CO2 storage, Geochim. Cosmochim. Acta 81 (2012) 28–38.

[36] P. Naeiji, T.K. Woo, S. Alavi, R. Ohmura, 2019, Interfacial properties of hydrocarbon/water systems predicted by molecular dynamic simulations, J. Chem. Phys. 150 (2019), 114703, https://doi.org/10.1063/1.5078739.

[37] A.K.N. Nair, M.F.A.C. Ruslan, M.L.R. Hincapie, S. Sun, 2022, Bulk and interfacial properties of brine or alkane in the presence of carbon dioxide, methane, and their mixture, Ind. Eng. Chem. Res. 61 (2022) 5016–5029, https://doi.org/10.1021/acs.iecr.2c00249.

[38] V. Mirchi, M. Dejam, V. Alvarado, Interfacial tension and contact angle measurements for hydrogen-methane mixtures/brine/oil-wet rocks at reservoir conditions, Int. J. Hydrog. Energy 47 (82) (2022) 34963–34975, https://doi.org/10.1016/j.ijhydene.2022.08.056.

[39] G. Zhang, T. Chen, F. Wang, B. Sun, Y. Wang, D. Hou, Experimental determination of deviation factor of natural gas in natural gas reservoir with high CO2 content, E3S Web Conf. 245 (2021) 01045, https://doi.org/10.1051/e3sconf/202124501045.

[40] L.N. Legoix, L. Ruffine, J. Donval, M. Haekel, 2017, Phase equilibria of the CH4-CO2 binary and the CH4-CO2-H2O ternary mixtures in the presence of a CO2-rich liquid phase, Energies 10 (12) (2017) 2034, https://doi.org/10.3390/en10122034.

[41] E. Moioli, R. Mutschler, A. Züttel, 2019, Renewable energy storage via CO2 and H2 conversion to methane and methanol: assessment for small scale applications, Renew. Sustain. Energy Rev. 107 (2019) 497–506, https://doi.org/10.1016/j.rser.2019.03.022. ISSN 1364-0321.

[42] M. Szuhaj, N. Ács, R. Tengölics, A. Bodor, G. Rakhely, K.L. Kovacs, Z. Bagi, 2016, Conversion of H2 and CO2 to CH4 and acetate in fed-batch biogas reactors by mixed biogas community: a novel route for the power-to-gas concept, Biotechnol. Biofuels 9 (2016) 102, https://doi.org/10.1186/s13068-016-0515-0.

[43] M. Kanaani, B. Sedaee, M. Asadian-Pakfar, 2022, Role of cushion gas on underground hydrogen storage in depleted oil reservoirs, J. Energy Storage 45 (2022), 103783, https://doi.org/10.1016/j.est.2021.103783. ISSN 2352-152X.

[44] A. Iulianelli, S. Liguori, J. Wilcox, A. Basile, Advances on methane steam reforming to produce hydrogen through membrane reactors technology: a review, Catal. Rev. 58 (1) (2016) 1–35, https://doi.org/10.1080/01614940.2015.1099882.

[45] S. Plimpton, 1995, Fast parallel algorithms for short-range molecular dynamics, J. Comp. Phys. 117 (1995) 1–19.

[46] A.R. Leach, Molecular modelling: Principles and applications, chapter 3: Empirical force field models: molecular mechanics, Addison Wesley Longman Limited, 1996, pp. 196–204.

[47] M.P. Allen, D.J. Tildesley, 2017, Computer Simulation of Liquids, 2nd ed., Oxford University Press, Oxford, 2017.

[48] H.J.C. Berendsen, J.R. Grigera, T.P. Straatsma, 1987, The missing term in effective pair potentials, J. Phys. Chem. 91 (24) (1987) 6269–6271.

[49] J.L.F. Abascal, C. Vega, 2005, A general purpose model for the condensed phases of water: TIP4P/2005, J. Chem. Phys. 123 (2005), 234505, https://doi.org/10.1063/1.2121687.

[50] J.G. Harris, K.H. Yung, Carbon dioxide's liquid-vapor coexistence curve and critical properties as predicted by a simple molecule model, J. Phys. Chem. 99 (12021) (1995) 1995.

[51] W.L. Jorgensen, D.S. Maxwell, J. Tirado-Rives, 1996, Development and testing of the OPLS all-atom force field on conformational energetics and properties of organic liquids, J. Am. Chem. Soc. 118 (1996) 11225.

[52] Q.Y. Yang, C.L. Zhong, Molecular simulation of adsorption and diffusion of hydrogen in metal-organic frameworks, J. Phys. Chem. B 109 (2005) (2005) 11862–11864, https://doi.org/10.1021/jp051903n.

[53] S. Liu, X. Yang, Y. Qin, Molecular dynamics simulation of wetting behavior at CO2/water/solid interfaces, Chin. Sci. Bull. 55 (21) (2010) 2252–2257, https://doi.org/10.1007/s11434-010-3287-0.

[54] K. Ofori, C.M. Phan, A. Barifcani, S. Iglauer, An investigation of some H2S thermodynamical properties at the water interface under pressurized conditions through molecular dynamics, Mol. Phys. (2021), https://doi.org/10.1080/00268976.2021.2011972.

[55] Y. Yang, K. Narayanan, S. Sun, 2017, Molecular dynamics simulation study of carbon dioxide, methane and their mixture in the presence of brine, J. Phys. Chem. B 121 (2017) 9688–9698. https://doi.org/10.1021/acs.jpcb.7b08118.

[56] J.P. Ryckaert, G. Ciccotti, H.J. Berendsen, Numerical integration of the cartesian equations of motion of a system with constraints: molecular dynamics of n-alkanes, J. Comput. Phys. 23 (1977) 327–341, https://doi.org/10.1016/0021-9991(77)90098-5.

[57] Y. Weinbach, R. Elber, 2005, Revisiting and parallelizing SHAKE, J. Comput. Phys. 209 (1) (2005) 193–206.

[58] V.K. Shen D.W. Siderius W.P. Krekelberg H.W. Hatch Eds., NIST Standard Reference Simulation Website, NIST Standard Reference Database Number 173, National Institute of Standards and Technology, Gaithersburg MD, 20899, http://doi.org/10.18434/T4M88Q.

[59] J.G. Kirkwood, F.P. Buff, 1949, The statistical mechanical theory of surface tension, J. Chem. Phys. 17 (1949) 338–343, https://doi.org/10.1063/1.1747248.

[60] J. Alejandre, D.J. Tildesley, G.A. Chapela, 1995, Molecular dynamics simulation of the orthobaric densities and surface tension of water, J. Chem. Phys. 102 (1995) 4574, https://doi.org/10.1063/1.469505.

[61] Y. Yang, M.F.A. Ruslan, A.K. Nair, S. Sun, 2019, Effect of ion valency on the properties of the carbon dioxide–methane–brine system, J. Phys. Chem. B 123 (12) (2019) 2719–2727, https://doi.org/10.1021/acs.jpcb.8b12033.